III nitrides and UV detection

2001 J. Phys.: Condens. Matter 13 7115

(http://iopscience.iop.org/0953-8984/13/32/316)

INSTITUTE OF PHYSICS PUBLISHING JOURNAL OF PHYSICS: CONDENSED MATTER

J. Phys.: Condens. Matter **13** (2001) 7115–7137 PII: S0953-8984(01)24819-X

III nitrides and UV detection

E Muñoz[1], E Monroy[1], J L Pau[1], F Calle[1], F Omnès[2] and P Gibart[2]

[1] ISOM–IEL, ETSI Telecomunicación, C Universitaria, Universidad Politécnica de Madrid, 28040 Madrid, Spain
[2] CRHEA–CNRS, Parc Sophia Antipolis, rue Bernard Gregory, 06560 Valbonne, France

Received 14 May 2001
Published 26 July 2001
Online at stacks.iop.org/JPhysCM/13/7115

Abstract

III nitrides have become the most exciting challenge in optoelectronic materials in the last decade. Their intrinsic properties and an intense technological effort have made possible the fabrication of reliable and versatile detectors for short wavelengths.

In this work, materials and devices issues are considered to provide a full picture of the advances in nitride UV photodetection. First, basic structures like photoconductors, Schottky, p–i–n and metal–semiconductor–metal photodiodes and phototransistors are compared, with emphasis on their specific properties and performance limitations. The efforts in the design and fabrication of more advanced detectors, in the search for higher quantum efficiency, contrast, signal-to-noise or speed operation, are reviewed afterwards. Metal–insulator–semiconductor diodes, avalanche photodetectors and GaN array detectors for UV imaging are also described. Further device optimization is linked with present materials issues, mainly due to the nitride quality, which is a direct result of the substrate used. The influence of substrates and dislocations on detector behaviour is discussed in detail. As an example of AlGaN photodetector applications, monitoring of the solar UV-B radiation to prevent erythema and skin cancer is presented.

1. Introduction

The ultraviolet (UV) region of the electromagnetic spectrum has been paid increasing attention since the beginning of the 19th century. The Sun is the most powerful UV source, and the living species of the Earth's ecosystem are affected by the solar UV radiation, which is usually classified into three bands, UV-A (400–320 nm), UV-B (320–280 nm) and UV-C (below 280 nm). The ozone layer and other atmospheric gases strongly absorb the UV emission from the Sun, and only light with wavelengths longer than 280 nm reaches the Earth's surface. The determination of the effects of the various solar UV bands on the terrestrial ecosystem and on human beings is an important subject, and has been driving the need for reliable and efficient visible-blind UV detectors [1]. On the other hand, the measurement of man-made UV sources requires UV photodetectors with solar-blind characteristics (cut-off wavelength below 280 nm).

There is a wide range of applications and studies around the UV region, from UV astronomy, resin curing of polymeric materials, combustion engineering, water purification, flame detection and biological effects to more recent proposals like early missile plume detection, secure space-to-space communications and pollution monitoring. A variety of UV detectors are available, mainly Si-based photodetectors and photomultipliers (PMs). These standard solutions have significant limitations, either due to the need of filters to stop low energy photons (visible and IR light), their degradation and lower efficiency, or because of the need of a high voltage supply (PM case). The development of higher bandgap III arsenides or III phosphides for UV photodetectors has not progressed markedly [2].

To avoid the use of filters and achieve visible-blind operation, UV detectors based on wide bandgap semiconductors have been studied during the last decade. Thin film synthetic diamond ($E_g = 5.4$ eV—227 nm) detectors were developed and commercialized as polycrystalline or granular photoconductor devices. SiC pn junction photodetectors ($E_g = 2.9$ eV—433 nm) are also available. However, the turning point to make visible-blind UV detectors an appealing reality has been the development of (In, Al, Ga)N semiconductors [2].

III nitrides are direct bandgap materials, with GaN showing its absorption edge at 365 nm ($E_g = 3.4$ eV) and AlN at 200 nm ($E_g = 6.2$ eV), and with the ability to form heterojunctions. Even the 400 nm UV boundary can be obtained using (In, Ga)N alloys. This tunability of the detection edge by just varying the Al mole fraction, and the fact that (In, Al, Ga)N technology is already fully commercial for blue light emitting diodes (LEDs), are two important points that have made (Al, Ga)N alloys the most adequate solution for UV detection in many applications.

A detailed review on the developments of GaN UV photodetectors has been published recently [3]. Tracing back early developments, the photoconductive properties of GaN were studied by Pankove and Berkeyheiser in 1974 [4], and the first GaN UV photodetectors was reported by Khan *et al* in 1992 [5]. Since then, various teams have been exploring and developing virtually all types of photodetector structure. In these efforts, we may consider an initial exploratory phase, trying to confirm that GaN and AlGaN photodetectors (with low Al mole fractions) were feasible. In this period early publications came from the industrial side (Apa Optics). A second stage was focussed on developing high responsivity, true visible-blind photosensors, and medium Al mole fraction devices; and the current third stage points to solar-blind AlGaN photodetectors (higher Al mole fractions) and focal plane arrays. Such development steps reflect how technological difficulties are being overcome, and also the interests of the funding agencies. Photoconductive, p–n junction, p–i–n devices, Schottky barrier (SB), metal–semiconductor–metal (MSM) and metal–insulator–semiconductor structures (MIS), phototransistors, detector arrays, avalanche detectors etc have already been reported [3]. UV imaging using 8×8 Schottky barrier GaN arrays was demonstrated in 1997 [6]. Improvements in device speed have come together with the advances in the substrate quality, layer doping, ohmic contact technology and device design and fabrication. However, materials quality and processing steps are not yet mature, and a full industrial drive of AlGaN UV detectors still needs a further R+D effort during the forthcoming years.

The lack of appropriate substrates is a pending problem in the nitride device development. From the physics viewpoint, photodetectors work under very low currents and very low photon fluxes, and they reflect even more pronouncedly some of the current problems in AlGaN layer quality. Dislocations seem not be so harmful for LED operation except at high current densities, and traps are blamed for large signal switching problems in AlGaN/GaN high electron mobility transistors (HEMTs). Both families of devices operate at significant current densities, and free carriers screen some of the effects shown up in UV photodetectors. However, in AlGaN layers, slow trapping processes are usually present at very low currents, giving rise

to persistent photoconductivity effects (PPC). This PPC is not yet fully understood, and it may show up in AlGaN photodetector devices, depending on their contact structure, materials quality and device operation. Basically, the characteristics and limitations in present AlGaN UV photodetectors are directly dependent on the quality of the (Al, Ga)N epitaxial layers achieved today.

In this article, the development and progress of AlGaN photodetectors are reviewed, trying to guide the reader through the main achievements during the last decade. The behaviour of the various basic structures will be first described, trying to summarize their characteristics and limitations. Some developments linked to specific applications will be presented, along with the results derived from the use of various substrates. Recent achievements have pointed to the fabrication of photodetectors with rather high Al mole fractions, with emphasis on solar-blind devices, high speed structures, avalanche photodiodes and UV imaging technology. New results on the use of Si(111) substrates are included. Finally, some materials issues, current problems and the physics learned from the photodetector activity will be discussed.

2. AlGaN epitaxial layers

As in most of the blue LED developments, efforts on GaN UV detectors have been focalized on the use of sapphire substrates and metal–organic vapour phase epitaxy (MOVPE) epitaxial technology. Only a few reports describe the fabrication of photodetectors using molecular beam epitaxy (MBE). GaN layers grown by epitaxial lateral overgrowth (ELOG) or by hydride vapour phase epitaxy (HVPE), Si (111) and even SiC substrates have also been utilized for detector fabrication. Regarding the detector layer fabrication, various schemes of buffer layers have been described to minimize dislocation density, although the buffer composition is predetermined in back illuminated devices.

In this chapter we will not run into materials growth details, although we summarise here some of the AlGaN growth details at CRHEA–CNRS and at ISOM–UPM, aiming to provide background information for the UV detector characteristics presented later. Details on the growth conditions for both epitaxial techniques have already been reported [7, 8].

At CRHEA, the growth of AlGaN layers on *c*-oriented sapphire substrates was performed by LP-MOVPE, using pure hydrogen as carrier gas, and trimethylaluminium, trimethylgallium and purified ammonia as precursors. GaN or AlGaN epilayers were grown on top of thin, low temperature grown GaN or AlN nucleation layers. AlGaN growth temperatures were typically 20–40 °C higher than the growth temperatures currently used for GaN ($T = 1140\,^{\circ}\mathrm{C}$). Typical growth rates of AlGaN alloys lie in the 0.9–1.2 $\mu\mathrm{m\,h^{-1}}$ range. n-type doping (Si) was performed using a silane source. The Al mole fraction was determined by energy dispersion spectroscopy (EDS) or by x-ray double diffraction measurements (XRD). For Al mole fractions of 0.35 a typical full width at half maximum (FWHM) of about 670 arc seconds has been measured for the (0002) diffraction peak in the $\theta/2\theta$ configuration, and it can be compared with a FWHM of 300 arc seconds currently measured under the same conditions in GaN epilayers. The energy bandgap and the absorption coefficient at room temperature of the MOVPE layers (compressive strain) have been determined by optical transmission measurements and photothermal deflection spectroscopy (PDS). These are key parameters for photodetectors, and establish a kind of reference for the detection cut-off wavelength and for the device response below the bandgap (figure 1). For low Al mole fractions, a bowing parameter of 0.8 eV is observed, in contrast with the downward bowing parameter of 1.3 eV reported by Brunner *et al* [9]. Low temperature photoluminescence shows no low energy transitions related to residual acceptors were observed in the 3.2–3.4 eV range. As an example, for layers with 7% of Al, the near-edge excitonic peak (most probably a donor-bound exciton) is located at 3.685 eV,

and its FWHM is 18 meV. The electrical properties of AlGaN layers were measured at room temperature by the Hall effect. Undoped AlGaN samples were insulating. Silicon-doped GaN and $Al_{0.22}Ga_{0.78}N$ epilayers, with n-type doping levels of 5×10^7 cm^{-3} and 2×10^{18} cm^{-3} showed typical mobilities of 180 cm^2 V^{-1} s^{-1} and 50 cm^2 V^{-1} s^{-1} respectively.

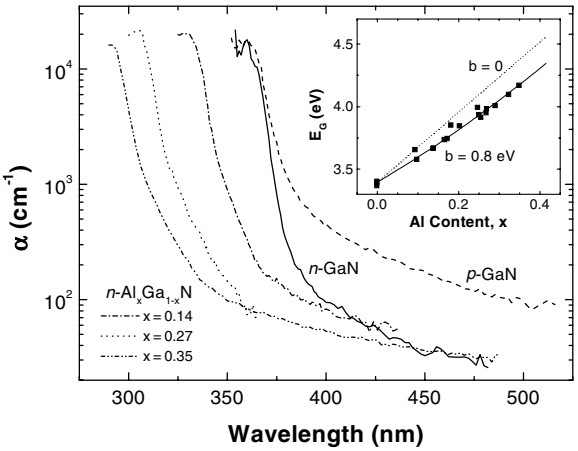

Figure 1. Absorption coefficient of n-$Al_xGa_{1-x}N$ and p-GaN measured by PDS. In the inset, variation of the bandgap energy with Al mole fraction (after [21]).

The growth at ISOM–UPM of AlGaN films on Si(111) substrates was performed by GS-MBE, using a radio frequency (RF) plasma source to activate the nitrogen, and conventional Knudsen cells for the rest of the elements (Ga, Al and Si). One the goals of this technology was to obtain low cost UV detectors, because the price per cm^2 may reach a factor of ten lower for Si than for sapphire material. High quality AlGaN layers were grown at 770 °C with Al contents ranging from 10% to 76%, using high temperature (800 °C) AlN buffer layers. The RHEED pattern showed a sharp $\times 2$ surface reconstruction along the growth, characteristic of a 2D growth mode, leading to smooth surface morphologies. The *in situ* interferometry measurements indicated a growth rate around 0.55 μm h^{-1}. Due to the lower deposition temperatures in comparison with MOCVD growth, cracking problems were not observed in any sample up to 2 μm thick. The Al mole fraction was estimated by x-ray double diffraction (XRD) measurements, and it follows a linear relationship with the Al flux (beam equivalent pressure). Typical values of FWHM from XRD data were 8.5 and 15 arc minutes for GaN and AlGaN ($x = 0.30$) layers respectively, with thickness between 0.5 and 2 μm. The residual n-type doping was around 1×10^{17} cm^{-3}, according to C–V measurements. Photoluminescence spectra were dominated by a peak which is attributed to the donor-bound exciton. Yellow band emission was not observed, indicating a very low contamination level in the MBE samples. The dependence of the energy bandgap on the Al content indicates a downward parameter similar to that of Brunner *et al* [9]. Electrical characterization of the layers by Hall effect provides mixed information, due to the interdiffusion between Si atoms from the substrate and group III species from the epilayer.

3. UV photodetectors: basic structures

Figure 2 schematizes the basic photodetector structures fabricated with AlGaN layers. Technological and device characterization details will usually not be provided here. Results

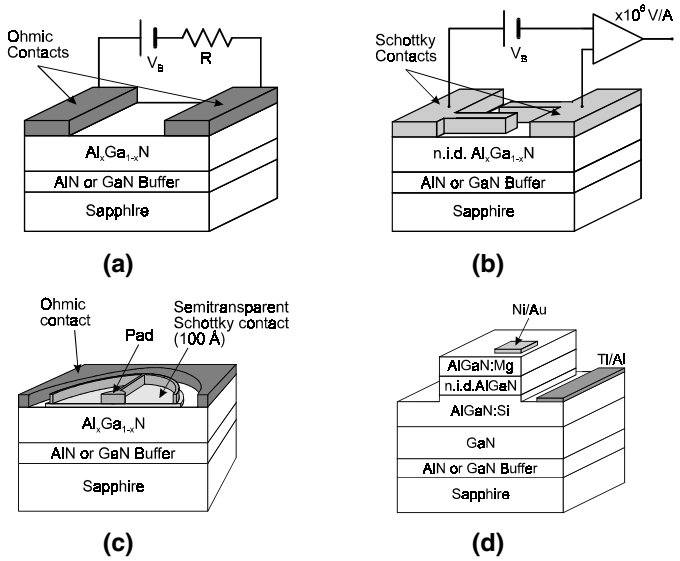

Figure 2. Schematic structure of (a) AlGaN photoconductors, (b) MSM photodiodes, (c) Schottky barrier photodetectors and (d) p–i–n photodiodes.

for the basic photodetector structures will be presented, in order to illustrate the main steps in the developments, and to discuss materials and processing issues.

Photodetector parameters described in textbooks are applicable here to UV sensors: quantum efficiency (η), responsivity (R), power linearity, spectral response, bandwidth (BW), noise equivalent power (NEP), detectivity (D^*), etc. Detectivity ($D^* = \sqrt{A_{opt}}\mathrm{BW/NEP}$, where A_{opt} stands for the effective optical area) is a figure of merit quite adequate for performance comparison [10]. Because of the emphasis on the insensitivity of AlGaN detectors to longer wavelength photons, another figure of merit is linked to the ratio between the peak responsivity and that below the bandgap, that is, the UV/visible contrast. It reflects the abruptness of the detection edge and the presence of gap states, both indicative of the quality of the layer. As used in electrical filters, it can be more precisely defined as the number of nm needed to reduce the responsivity by a decade. Another important point is the photocurrent gain, reflecting the effective number of carriers collected by the detector external circuit per internally photogenerated hole–electron pair. Carrier multiplication and photoconductive gain are two mechanisms that can be present in semiconductor photodetectors. Regarding noise, as in most semiconductor devices, the low frequency noise of AlGaN photodetectors is $1/f$ limited, while at high frequencies other noise sources are present, depending on the structure and operating point (thermal noise, shot noise etc). Very low dark currents are always advisable regarding noise properties.

3.1. Photoconductors

Photoconductive detectors have early attracted much interest because of their simplicity and high responsivity, and they are potential candidates for low cost monitoring applications (flame and fire detection) [1, 3–5, 11–13]. Photoconductivity in GaN is usually associated with slow, non-linear processes, significant photoresponse for photons below bandgap and temperature dependent characteristics. Because of its link with carrier trapping, photoconductivity and

recombination kinetics studies were also related to the yellow emission and to other below-the-bandgap GaN luminescence properties [14–16].

As will be discussed later, the strong influence of materials quality and resistivity on the real properties of nominal ohmic contacts originated a very large dispersion in early studies. Difficulties in achieving good ohmic contacts in AlGaN layers meant that many photoconductivity detectors reported in the literature were in fact a kind of hybrid between a photoconductor and a couple of back-to-back SBs (Schottky MSM).

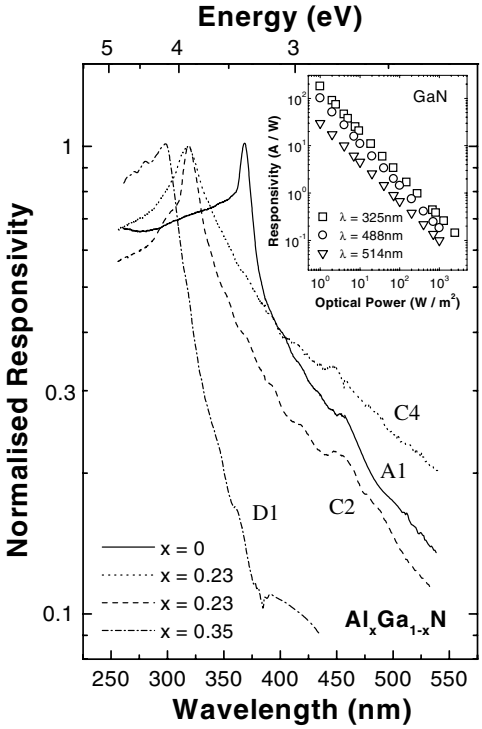

Figure 3. Normalized spectral responsivity of samples with different Al contents and Si doping (A1: n.i.d., C2: $N_D = 6.1 \times 10^{17}$ cm^{-3}, C4: 1.7×10^{18} cm^{-3}, D1: 2.0×10^{18} cm^{-3}) (after [13]).

Figure 3 plots the spectral responsivity of AlGaN photoconductors with different Al contents, using Ti/Al ohmic contacts on Si-doped or on non-intentionally doped layers. It is a clear example showing how the Al mole fraction shifts the detection edge. AlGaN photoconductors show a very high dc responsivity that is dependent on the incident power (P). The inset to figure 3 shows that it decreases approximately as $P^{-0.85}$, over five decades. The peak of the spectra is assigned to the absorption superposition of the A and B excitons. This peak is located at 319 nm in samples with $x = 0.22$. All samples present a significant response below bandgap, and suffer from PPC effects [13]. Good visible-blind devices are not obtained so far. As shown in figure 4, the detectors show extremely slow and non-exponential transient responses, which are responsible for their frequency dependent ac responsivity. The importance of the tunnel recombination, which increases with time and dominates the response even in the undoped sample, is shown in the inset.

These results support the presence of a photoconductive gain mechanism. The standard model for such an effect is described in terms of a long hole trapping time that causes a minority recombination time much longer than the electron transit time [10]. Although this

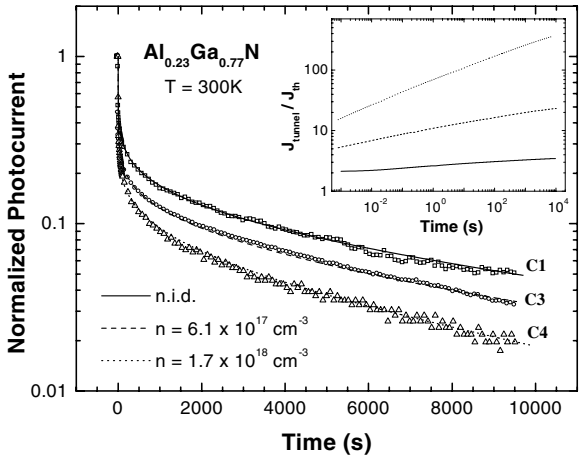

Figure 4. Normalized photocurrent decays of $Al_{0.23}Ga_{0.77}N$ photoconductors, after an excitation light pulse from an He–Cd laser, and their computer simulation. Inset: evolution of the tunnel:thermionic current ratio with time and Si doping (after [13]).

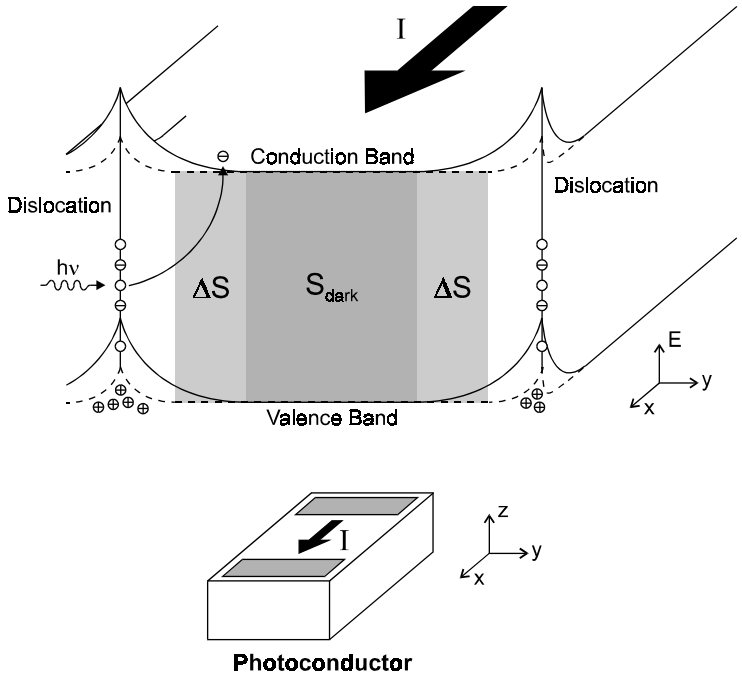

Figure 5. Diagram of the energy bands in a section of the photoconductor perpendicular to the current flux. Dashed lines indicate the changes of band-bendings around dislocations and due to illumination (after [19]).

mechanism may explain some low frequency gain present in AlGaN photodetectors [15, 16], the characteristics of GaN photoconductors can be better understood by a modulation of the effective sample conduction section, due to the changes in the space charge regions generated by the dislocations, as described in [17, 18]. This model also explains the high photoconductor

response below the bandgap. The levels responsible for visible absorption can be due either to point defects, such as dopants or vacancies, or to defects localized in lattice discontinuities (dislocations, grain boundaries and interfaces). If these defects are charged, they originate depletion regions around them, which reduce the effective conduction section of the device (figure 5). Under illumination, they are ionized, the net charge around the defects decreases, the associated space charge regions shrink and the effective conduction section of the device increases. This modulation of the effective conduction section may originate the PPC observed in this material below the gap. Thus, the defect-related space charge regions involved in the dc photocurrent mechanism cannot react as the chopper frequency increases. As shown in figure 6 for frequencies from 7 Hz to 700 Hz, the responsivity decreases markedly, its dependence on optical power tends to flatten and its below-the-gap response is lowered [19]. These results indicate that in characterizing photoconductive detectors, quantitative results depend on both materials parameters but also on the measurement details, explaining the dispersion of results found in the literature.

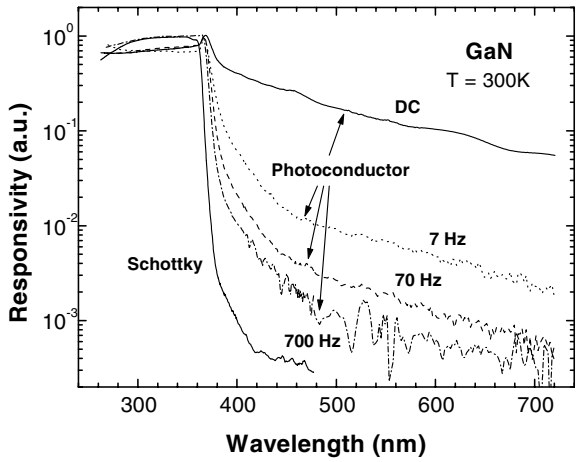

Figure 6. Normalized spectral response of a photoconductor measured with a lock-in technique and different chopping frequencies. The spectrum of a Schottky photodiode on the same sample is also shown for comparison (after [19]).

3.2. AlGaN photodiodes

To illustrate the unique property of AlGaN alloys that allows us to choose the detector cut-off wavelength *à la carte*, just by selecting the Al mole fraction, Schottky photodiodes were fabricated for a range of Al compositions [20]. A visible rejection of more than 10^3 is usually obtained (figure 7). The cut-off wavelength shifts with Al content from 362 nm ($x = 0$) to 295 nm ($x = 0.35$). As shown in the inset, the device photocurrent increases linearly with optical power in the whole measured range (10 mW m^{-2} up to 2 kW m^{-2}). Above-the-bandgap responsivities of 53.4, 44.9 and 29.4 mA W^{-1} were obtained for $x = 0.19$, 0.27 and 0.35, respectively.

Detector speed is usually determined by exciting with short (ns) laser pulses (typically $\lambda = 266$ nm), and by varying the external load resistor in a proper low capacitance high frequency electronics setup. Extrapolating results for zero external resistance an estimation of the device internal delay response is obtained. It was found that the time response of these Schottky photodiodes was *RC* limited [20].

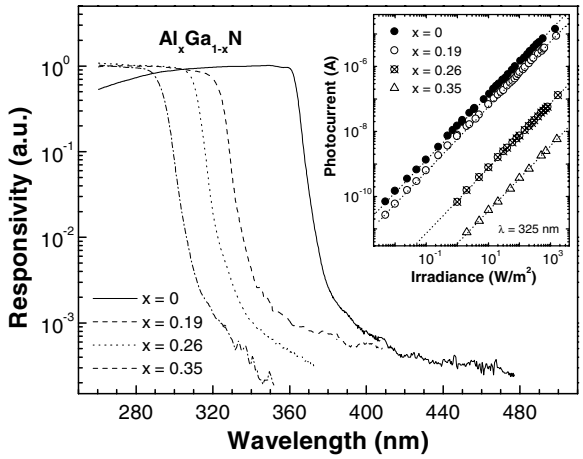

Figure 7. Spectral response of n-$Al_xGa_{1-x}N$/Au Schottky photodiodes, measured at room temperature. In the inset, photocurrent against irradiance at 325 nm (after [7]).

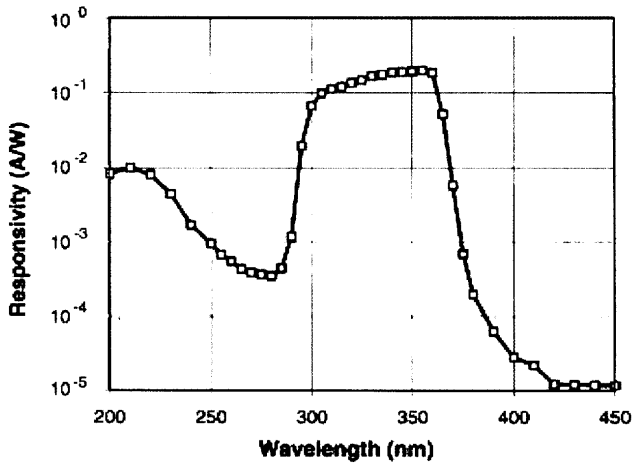

Figure 8. Spectral response of a GaN/AlGaN photodiode, limited by the absorption edge of GaN at 365 nm and by the AlGaN ($x = 0.28$) absorption, producing a window response (after [27]).

In the above Schottky barrier photodiodes, the $1/f$ noise properties were studied. By integrating in the equivalent bandwidth determined by the RC product of the photodiode, the noise equivalent power (NEP) was estimated in the 10^{-8} W range. Detectivities of 1.2×10^7 mHz$^{1/2}$ W^{-1} are obtained in $Al_{0.22}Ga_{0.78}N$/Au detectors at -2 V bias, and they increase up to 3.5×10^7 mHz$^{1/2}$ W^{-1} for -1.35 V bias. A computer analyses of these devices has been presented by Monroy *et al*, showing the dependences between materials parameters and device characteristics [21]. The compromises and alternatives for detector design are also shown in this publication.

AlGaN p–n and p–i–n photodiodes show the same qualitative behaviour as Schottky photodiodes concerning responsivity, contrast, linearity, time response, low frequency noise etc. Photocurrent scales linearly with optical power, and a sharp cutoff with a UV/visible contrast larger than 10^3 is typically obtained. Detectivities are usually higher than in Schottky

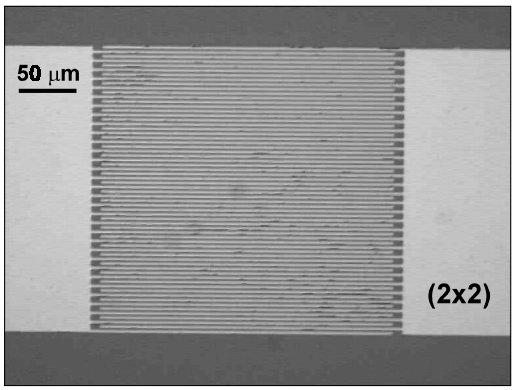

Figure 9. Photograph of an MSM photodetector, which consists in two interdigitated Schottky barrier electrodes. In this case, finger widths and gap spacings are 2 μm, extended over an active area of 250 × 250 μm^2.

photodiodes, mainly due to their lower dark currents. Since the early reports, depending on the specific design, responsivity usually increases significantly at reverse voltages in Schottky and p–n photodetectors, indicating that some photoconductive effects may appear [22]. The difficulties in obtaining a low resistivity p-type region and good ohmic contacts produce devices with high series resistances. Standard devices may show low photocarrier collection efficiency, due to a limited lateral and vertical diffusion length, and to the high resistivity of the p-type contact.

A common feature of AlGaN p–i–n photodiodes is a significant decrease of the responsivity for photon energies above the bandgap, leading to a short wavelength cutoff [23–26]. Carriers photogenerated close to the surface have to diffuse towards the junction to be collected. At shorter wavelengths the absorption becomes more superficial, many more carriers recombine before reaching the junction and the responsivity above bandgap decreases. The use of an $Al_xGa_{1-x}N$ optical window results in an enhancement of the peak responsivity. The AlGaN window layer behaves like a long pass filter, and a narrow band photodetector is formed (figure 8).

3.3. Metal–semiconductor–metal photodiodes

Due to its bandwidth and low fabrication costs, MSM devices are always very attractive photodetector structures. Schottky MSM devices are based on two rectifying contacts, back-to-back [27–30]. For that objective, high resistivity, non-intentionally doped (n.i.d.) material is required. This results in very low leakage currents, and thus good noise characteristics. To illustrate AlGaN MSM behaviour, some results are presented below. Insulating LPMOVPE $Al_xGa_{1-x}N$ ($0 \leqslant x \leqslant 0.25$) epilayers were used. Detectors consisted of two interdigitated Schottky barrier electrodes on a planar structure, with finger widths and gap spacings of 2, 4 and 7 μm, in an active area that may range from 250 × 250 μm^2 to 1 × 3 mm^2 (figure 9).

Figure 10 shows the spectral response of AlGaN MSM photodiodes at different bias. The responsivity is quite flat above the bandgap, with a sharp cutoff wavelength that shifts to shorter wavelengths with increasing Al content. Photocurrent scales linearly with the optical power, independently of bias. A visible rejection of four to five orders of magnitude is obtained at 5 V or higher voltages. The UV/visible contrast decreases by one decade when bias is reduced, remaining at $\sim 10^3$. For excitations over the bandgap a gain mechanism or superlinear response

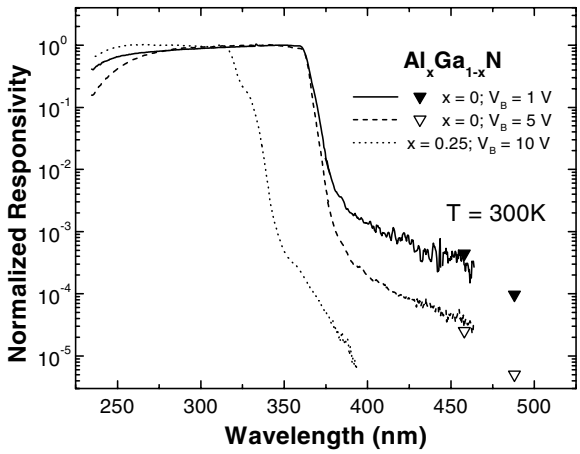

Figure 10. Spectral response of $Al_{0.25}Ga_{0.75}N$ and GaN MSM photodiodes, measured at different bias.

is present at biases over 2 V. The presence of sublinear or superlinear responses at certain bias in MSM devices has been reported by several groups [28, 30, 31].

Concerning their time response, photocurrent decay measurements indicate that the minimum response time of the above devices is quite far below 10 ns, and either a *RC* or a carrier transit time limit is estimated to be in the picosecond range. At 28 V bias, an NEP$^* \sim 24 \times 10^{-12}$ W Hz$^{-1/2}$ was measured in $Al_{0.25}Ga_{0.75}N$ photodiodes, that corresponds to $D^* = 2.3 \times 10^{10}$ W^{-1} Hz$^{1/2}$ cm [29].

3.4. AlGaN phototransistors

Both GaN bipolar and field effect phototransistors (FETs) have been reported [32, 33]. They follow a basic behaviour, with the light entering through the substrate (sapphire, back illumination), passes an optical window layer (n-type AlGaN, usually), to reach either the base-collector space charge region or the GaN channel. Photocarriers are quickly driven towards the contacts, and amplification is obtained by the transistor action. In bipolar devices the base may be left floating. Large gains have been reported in both types of device, as high as 3000 A W^{-1}, and PPC effects are usually present.

4. UV detectors: advanced structures

As indicated in the introduction, high performance AlGaN/GaN UV detectors have recently been developed. True solar-blind operation, high quantum efficiency, low noise, higher speed etc, have been pursued. As a reference for the reader, ideal responsivities (quantum efficiencies of unity) would be 294 mA W^{-1} at 365 nm, and 161 mA W^{-1} at 200 nm. Solar blindness (detector cutoff below 280 nm) and UV/visible contrasts larger than four orders of magnitude have been achieved recently in various structures, reflecting the improvements in materials quality. Very low noise operation is clearly linked to very low dark currents, and significantly improved p–i–n, Schottky MSM and metal–insulator–semiconductor (MIS) structures have been presented. In fact, the development stages in nitrides UV detectors are marked by cut off wavelengths and detectivities that have evolved from the 360 nm border and the 10^7 cm Hz$^{1/2}$ W^{-1} range, respectively, to the 225 nm and the 10^{13} cm Hz$^{1/2}$ W^{-1} frontiers,

respectively. Devices with fast internal gain are of great interest, and avalanche gain has started to be studied in GaN photodetectors. A new era of UV imaging has clearly been opened by GaN-based detector arrays.

4.1. AlGaN p–i–n photodiodes

One of the objectives in some recent developments relate to achieve true solar-blind operation and high quantum efficiencies, and to use device designs that would allow focal plane arrays. P–i–n devices are usually preferred, and they illustrate the difficulties that were faced. High quality, higher Al mole fractions ($\geqslant$0.4), with good n- and p-type conductivity layers and ohmic contacts are required. The use of higher Al mole fractions implies new difficulties in the ohmic contact technology, and higher series resistances are usually obtained.

Solar-blind operation can be achieved using absorbing layers with Al mole fractions in the 40% range. Because of lattice mismatch problems, cracks in the layers are usually present. For the p-type region, such compositions pose a severe problem to really achieve p-type conduction and ohmic contacting. High resistivity layers are usually obtained. At shorter wavelengths, photons are absorbed very close to the surface, and surface problems, band-bending effects, and electric field crowding problems (non-uniform spatial variations) tend to be present. To minimize such effects, the thinning of the p-type AlGaN, and the use of a semitransparent metal contact (Ni/Au) on top, to collect carriers more efficiently and to lower the series resistance, have been used by the University of Texas–Austin [34]. In general, improvements in ohmic contacts to the p-type AlGaN layer are obtained by contacting on a p^+-GaN layer deposited on the p-type AlGaN region.

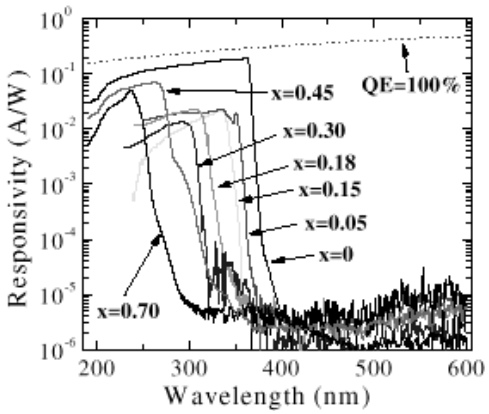

Figure 11. Spectral responses of $Al_xGa_{1-x}N$ p–i–n photodiodes. The dotted line represents the theoretical limit for an external quantum efficiency of 100% (after [35]).

Another route was followed at Northwestern University by developing p-type layers with higher Al mole fractions (up to 70%), and hence good optical windows were obtained in p–i–n structures [35]. By controlling the Al composition in the active region, peak responsivities in the 362 to 225 nm were reported. Such devices showed an UV/visible contrast up to six orders of magnitude, and peak responsivities of 0.20 A W^{-1} at 262 nm were obtained without applied bias (figure 11). Front and back illuminated structures were developed. A similar structure has been reported by Brown *et al* [36], with an n-type $Al_{0.64}Ga_{0.36}N$ window and an absorbing layer with 0.47 Al mole fraction. A responsivity of 51 mA W^{-1} at 273 nm was achieved. Solar-blind front- and back-side illuminated photodiodes have been demonstrated

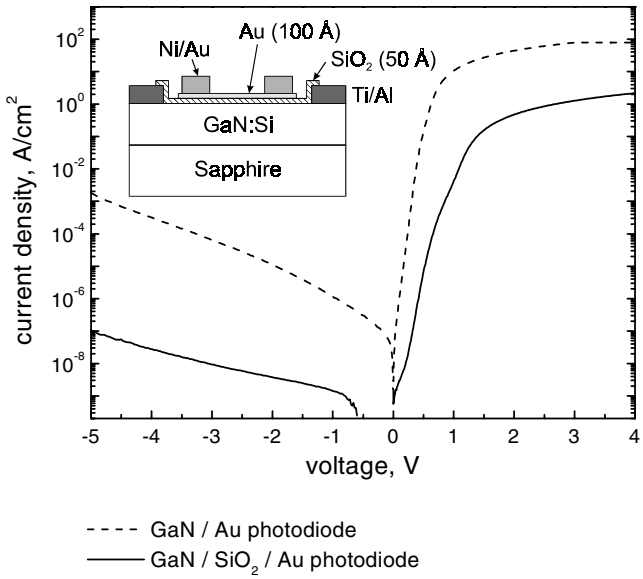

Figure 12. Dark current density against voltage in GaN/SiO_2/Au photodiodes compared with identical devices without the SiO_2 layer, fabricated on the same sample. In the inset, schematic structure of GaN/SiO_2/Au photodiodes (after [41]).

using an inverted heterostructure photodiode, an interesting approach where the wide bandgap absorbing layer is surrounded by narrower GaN p- and n-type thin contact layers [37]. In this scheme, the heterojunction band offsets block the diffusion of photoexcited carriers from the narrower bandgap layers into the active layer, and a peak responsivity of 80 mA W^{-1} at 285 nm is obtained.

4.2. Metal–semiconductor–metal photodiodes

As indicated previously, Schottky MSM devices offer various potential advantages, related to n.i.d. or n-type doping only requirements, fabrication simplicity and high speed operation. Their intrinsic very low dark currents lead to very low noise device characteristics. Solar-blind MSM devices have been reported, which combine high quantum efficiency and high speed operation. In fast devices reported by Carrano *et al* [38] it is claimed that the device speed is linked to carrier transit time characteristics, and not to the usual device *RC* limitations. This work proposes that the true bandwidth of the devices is dominated by the slower collection of holes, which may halve the intrinsic device speed if limited by electron transit time. Back-illuminated high performance devices were reported by Yang *et al*, where photons reach the $Al_{0.45}Ga_{0.55}N$ absorbing layer after passing through an optical window (60% of Al) followed by an AlGaN transition region. Passivated devices and Ti/Pt Schottky fingers lead to very low dark currents, with a responsivity peak of 0.1 A W^{-1} at 262 nm [39]. It was claimed that no or little photoconductive gain was present.

By using a double low temperature AlN buffer layer, Pernot *et al* have reported the growth of AlGaN layers with lower dislocation densities, and aiming at detector applications [40]. Very low dark currents in MSM devices, and a reduction of the PPC effects were observed.

4.3. Metal–insulator–semiconductor photodiodes

The need for very low dark currents has been brought by applications where very low optical powers are involved, flame detection being an important case. Photodetector leakage current is linked to layer quality, device design and processing details. New low noise and low dark current devices have been fabricated by Monroy *et al* by using a metal–insulator–semiconductor (MIS) structure [41]. The insertion of a thin SiO_2 layer at the metal–semiconductor interface results in a significant decrease of the dark current density. A decrease of four orders of magnitude is obtained as compared with standard Au Schottky barrier photodiodes, and an increase of the detectivity by a factor of 50 is estimated, while the responsivity only decreases by 20%. The spectral response is not modified by the presence of the oxide layer in the range measured ($\lambda > 230$ nm). A schematic diagram of MIS photodiodes is shown in the inset of figure 12. A similar trend was observed for $Al_xGa_{1-x}N$ ($0 \leqslant x \leqslant 0.35$) devices [42]. The noise spectral density in MIS structures is lower by more than three orders of magnitude than in similar devices without the SiO_2 layer, and the normalized detectivity is higher by more than one order of magnitude (4×10^{11} cm W^{-1} $Hz^{-1/2}$).

4.4. Avalanche UV detectors

To obtain UV photodiodes with internal gain due to avalanche multiplication is a very challenging objective. This achievement will make GaN detectors a real alternative to PM tubes. As discussed in section 6, the gain obtained in some MSM structures and the large gain obtained by photoconductive effects are usually linked to lower speed behaviour. Avalanche multiplication gain is an alternative mechanism that is being explored in GaN detectors. Due to materials problems, issues related to breakdown spatial uniformity and photocurrent distribution are now key problems. Since the Si culture, microplasma formation was linked to the presence of defects and dislocations. McIntosh *et al* reported microplasma-free GaN avalanche photodiodes 37 μm in diameter, with a multiplication gain of 10, and that led to demonstration of ultraviolet photon counting with GaN [43]. Carrano *et al* have presented a GaN separate absorption, charge and multiplication avalanche photodiode, and multiplication factors greater than 25 have been obtained [44]. In devices of 25 μm in diameter no microplasma emissions were observed, although they were present in larger area devices. The magnitude of the electric field at breakdown was estimated as 3.5 MV cm^{-1}.

4.5. UV imaging

UV imaging via digital cameras has a number of applications ranging from flame sensing and missile detection to biological studies. A first 8×8 GaN Schottky barrier photodiode array was reported by Lim *et al* [6]. The pixels were fabricated as mesa-type semitransparent Pd barriers, using two levels of metals. Individual pixel detectors showed a responsivity of 50 mA W^{-1}. In this direction, significant achievements have been obtained by several laboratories. A 256×256 photoconductive GaN imaging array using metal–semiconductor–metal structure with 30 μm^2 pixels was presented by NASA [45]. More recently, a visible-blind UV digital camera with 32×32 pixels has been presented by Honeywell [46]. GaN/$Al_{0.2}Ga_{0.8}N$ p–i–n photodiodes were used, sensing radiation in the 320–365 nm band. Responsivity reached a peak of 0.2 A W^{-1}, and detectivities of $D^* = 6.1 \times 10^{13}$ cm $Hz^{1/2}$ W^{-1} were estimated, that are very large values for a semiconductor photodetector. A similar 32×32 array, with an $Al_{0.1}Ga_{0.9}N$ optical window was presented by Yang *et al* [47]. These UV arrays and camera are an important forward leap in the development of UV detection devices and systems based on III nitrides.

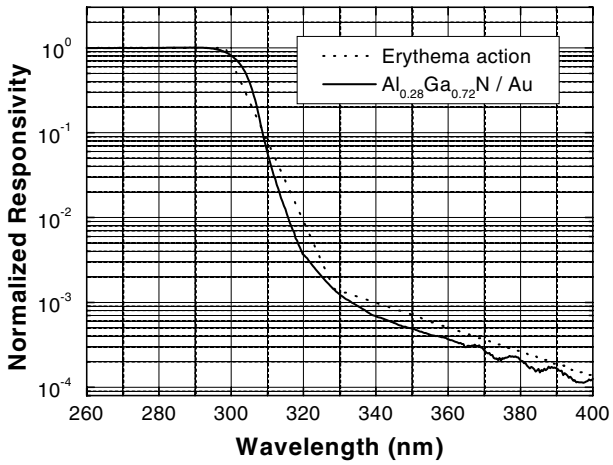

Figure 13. Spectral response of an AlGaN Schottky photodiode, compared with the CIE erythema action spectrum.

5. AlGaN photodetectors for biological applications

Although the lack of a major commercial drive to industrialize AlGaN detectors was stated before, the use of AlGaN UV detectors for erythema (skin sunburn) monitoring is a clear example of the advantages of this semiconductor family for UV monitoring.

There is presently a significant concern about the solar UV radiation, derived from the important effects of such wavelengths on the biological ecosystem. The biological action of the solar UV radiation has a strong dependence on the wavelength, and also depends on the specific biological process being under study (skin sunburn or erythema, DNA damage, plant damage, germicidal effects, bacteria killing, skin cancer etc) [2, 48, 49]. There are also well known cases where the UV exposure produces beneficial effects (UV therapy, vitamin D production etc), and again these positive UV effects are wavelength dependent. Because of its practical importance for human beings, the erythema (skin sunburning) action has been extensively studied and standarized by the Commission International de l'Eclarage (CIE). Such response is the most widely used UV biological action response, and its commercial solution is presently achieved by using narrow bandgap photodiodes (Si, GaAs, GaAsP). Thus a series of filters and phosphor coatings are inserted in the optical path, trying to match the erythema weight function. All these elements make the sensor system bulky, less reliable, need a temperature controlled chamber and prone to degradation. By proper materials and detector parameter design, the erythema weight action is approximated by a single AlGaN photodiode, without any filter, as shown in figure 13 [50]. This is one example of on-the-shelf commercial applications for AlGaN UV detectors.

6. Materials issues and detector behaviour

It has been already indicated that high performance AlGaN photodetectors are still a materials problem, a problem due to the quality of their absorbing layers. They are usually non-intentionally doped and with low carrier concentrations, and thus largely controlled by the electrical properties of the threading dislocations and other defects. Other technological difficulties with p-type doping and ohmic contacts also limit the detector performance, but they may not be so critical as in high current density devices.

At usual photocurrent levels, the dislocation problem is one of the most influential and unique in the nitride photodetector behaviour. In the present material, threading dislocations (10^8–10^{10} cm^{-2}) are not uniformly distributed. Single dislocations are anisotropic scattering centres, with extrinsic segregated impurities or point defects that create a band-bending and a depletion region around the dislocation. It is generally accepted that the dislocation lines have an acceptor behaviour, capturing electrons from the conduction band in an n-type region. Scanning capacitance microscope studies revealed the presence of negative charge in the vicinity of dislocations [51]. Ga vacancies in the core, or Ga vacancies complexed with oxygen would have an acceptor nature [52]. Neighbouring dislocations that form a sub-grain boundary or wall may now connect their space-charge regions to form an electronic barrier. These views have been used to model dislocation scattering and the carrier mobility collapse in GaN [53].

Carrier charging and discharging of carriers at dislocations is accompanied by a modulation of their associated space charge regions. Besides, photocapacitance studies in n-type layers have shown the presence of important hole trapping levels (a band, in fact), producing very slow processes [54]. Dislocations and point defects play an important role in AlGaN photodetector properties. They are considered to be responsible for PPC effects, reduced UV/visible contrast and low frequency gain and they are the main low frequency noise source because of the generated electron mobility fluctuations. Increasing optical power tends to saturate these traps, so their influence depends on incident power, becoming very important at low illumination powers and less important at high powers. Shallow levels and other defects seem also to modify the optical absorption edge abruptness, and an empirical Urbach potential can be obtained. The use of ELOG substrates and doped layers has alleviated but not avoided such effects. Photoconductivity is thus associated to internal gain, slow response and residual below-the-band response. Ohmic photoconductive detectors follow clearly such laws, and although various formalisms can be used, the physical view that photons help to modulated the effective conduction section of the detector (figure 5) seems to explain its huge dc gain at very low photon fluxes.

When considering Schottky barriers on nitrides, low ideality factors can been obtained, but significant tunnelling currents are usually present. Using a scanning current–voltage microscope, it has been recently shown that the reverse bias leakage current occurs at small isolated regions, primarily at dislocations with a screw component [55]. This same study shows that for a fixed dislocation density, the dislocation electrical activity is sensitive to local chemical and/or structural changes, which depend on growth conditions. Growth by MBE under Ga-rich conditions produced a reverse bias current density three orders of magnitude higher than in a sample grown under Ga-lean conditions. So it may be understood that growth stoichiometry influences the decoration of the dislocation cores [55]. Besides, threading dislocations having a screw component have been blamed as acting as strong nonradiative centres in GaN epitaxial layers [56]. It is experimentally found that, although Schottky barrier photodetectors working at zero bias do not show photoconductive gain, at reverse voltages photoconductive effects may be present, and a large increase of the responsivity (gain) with reverse bias is found. Photogenerated holes will tend to accumulate at the metal interface and to interact with the electrically active dislocations. It has also been suggested that polarization-induced surface and interface charges influence surface band bending. Schottky barriers on Ga and N faces have been shown to have different barrier heights [57]. Such surface properties have not been explored in relation to photodetector performance.

For both ohmic and Schottky contacts, reproducibility is easier if Si doped layers are used. Hence, in controlled resistivity layers clear photoconductive or Schottky barrier detector behaviour can be obtained by using the proper metals. When moving to non-intentionally

doped (n.i.d.), high resistivity layers, non-linear rectifying contacts are obtained. Thus we may talk about poor ohmic contacts, non-homogeneous Schottky barriers or low quality barriers. As an example, a p–n diode with poor ohmic contact at the p-type region becomes a sort of Schottky p–n device that under illumination induces anomalous photocurrent responses (negative currents) [58]. Thus, internal gains, non-linear responses, residual slow tails etc can be present in MSM and junction photodetectors under certain contact processing procedures.

It has been found experimentally that in MSM structures a clear cut between a pure photoconductive behaviour (good linear I–V characteristics) and back-to-back Schottky MSM characteristics is not found. A kind of *hybrid performance* can be obtained in n.i.d. and lightly doped AlGaN MSM devices in a reproducible way. In several published papers these characteristics have been described as fast photoconductors, or MSM devices with internal gain. On the other hand, it is true that, for example, in GaAs and InGaAs Schottky MSM photodetectors the presence of gain has also been reported even at low biases, indicating long lifetime trapping of photogenerated electrons or holes, and surface effects [59, 60]. Besides, electron accumulation in one of the contacts and hole accumulation in the cathode may modify the barrier height for hole and majority carrier injection. Photogenerated holes in the active region can become trapped at lattice or surface defects, and electrons can tunnel through the SB to maintain charge neutrality, thereby giving rise to low frequency gain. A more systematic study of this ohmic to Schottky MSM transition has been made by Misra and Moustakas [61] in GaN and by Pau *et al* [62] in AlGaN. In the first case, the resistivity of the GaN layer was changed by changing the III–V flux ratio during the MBE growth. The resistivity varied from 10 Ω cm to 10^7 Ω cm, the photoconductive gain changed by five orders of magnitude and the variation of the gain with excitation intensity (k exponent) was found to evolve from 0.5 to 1, as the resisitivity of the films increased. Although details of the layer structural and dislocation characteristics were not reported, as shown in [55] the electrical behaviour of dislocations is clearly affected by the growth stoichiometry conditions. A similar evolution from a slow photoconductive device to a fast Schottky MSM has been studied by Pau *et al* in AlGaN layers [62]. As illustrated in figure 14, for the same metal barrier, low Al mole fractions produce slow responses, and as the Al composition increases detectors become fast. Layer resistivity also increases, and the detector behaviour evolves from that of a pure ohmic photoconductor (responsivity depends on optical power with an exponent $k \cong 0.80$) towards a Schottky MSM behaviour ($k \cong 0.1$). As shown in figure 15 for a given Al mole fraction and two metal layer compositions, the higher barrier metal moves the device characteristics towards the Schottky barrier side. In these two studies [61, 62], both growth strategies (higher Al content and III/V ratio decrease) imply smaller size and higher misorientated hexagonal grains. The response in these *hybrid devices* could be dominated by a faster recombination at the grain edges through levels related to dangling bonds, acting as recombination centres. Thus, by controlling the layer resistivity and the metal barrier technology, an intermediate or hybrid device can be obtained in a reproducible way.

From the above considerations, the substrate becomes *a key issue* regarding materials quality and its influence on detector characteristics. This issue has run along several directions: on one hand, towards the higher quality side, with the use of ELOG, thick GaN templates, free standing layers, HVPE thick substrates or even bulk platelets. More systematic and conclusive comparisons have been made about the use of ELOG material. On the other hand, some experiments on SiC substrates have been reported, and the use of Si substrates has been more widely pursued.

Several laboratories have confirmed that detectors made using GaN layers grown on ELOG substrates showed a significant increase in responsivity and UV/vis contrast, while their reverse bias current decreased by orders of magnitude. Figure 16 exemplifies such a result for a simple

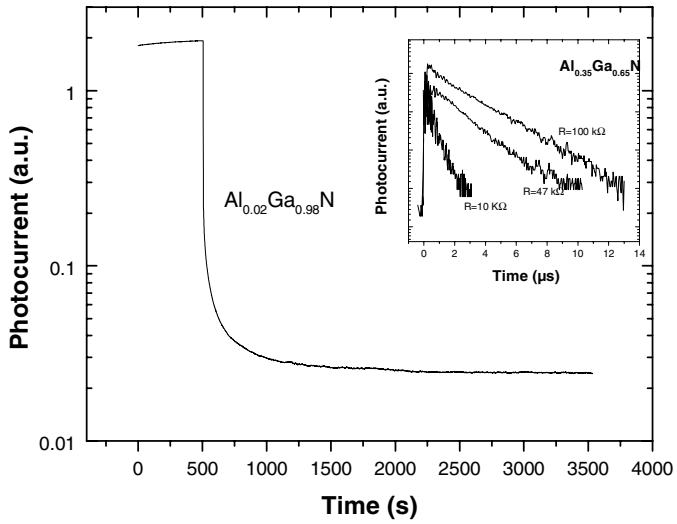

Figure 14. Temporal response of AlGaN ($x = 0.02$) MSM photodiodes grown on Si (111). Long non-exponential decays can be observed for low Al contents. The inset shows the fast exponential switch-off found for MSM with higher Al contents.

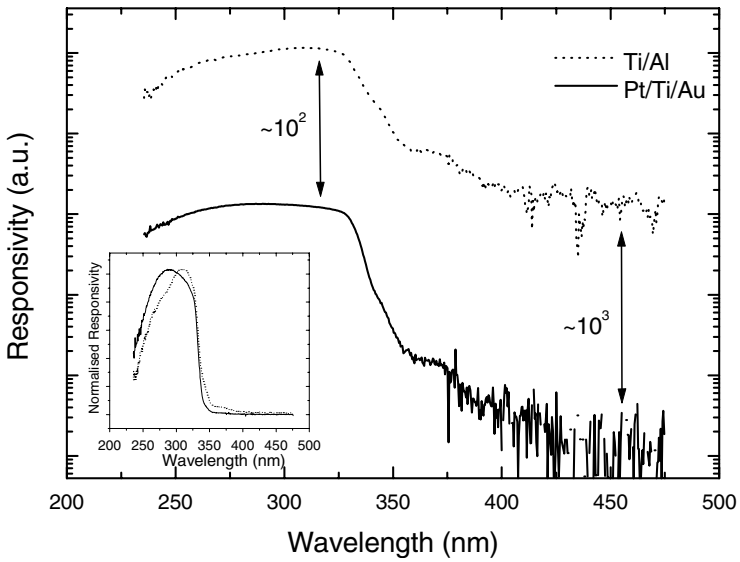

Figure 15. The spectral responses of AlGaN MSM photodetectors grown on Si (111) are shown in a logarithmic scale ($V_b = 5$ V). The dotted line corresponds to the Ti/Al contact system and the solid line to the Pt/Ti/Au system. The same curves in a linear scale are represented in the inset.

Schottky barrier GaN photodetector [63]. Solar-blind AlGaN p–i–n photodiodes have been grown by MOVPE on standard and on ELOG GaN layers on sapphire substrates by several laboratories. At UCSB they emphasized that although the peak responsivity of the detector on the dislocated GaN is comparable to that of the ELOG diodes (57 mA W^{-1} at 287 nm), its dark current is one order of magnitude higher, it shows a time response with a slow tail, and the spectral response is markedly different (figure 17) [64]. At NWU the two detectors exhibited

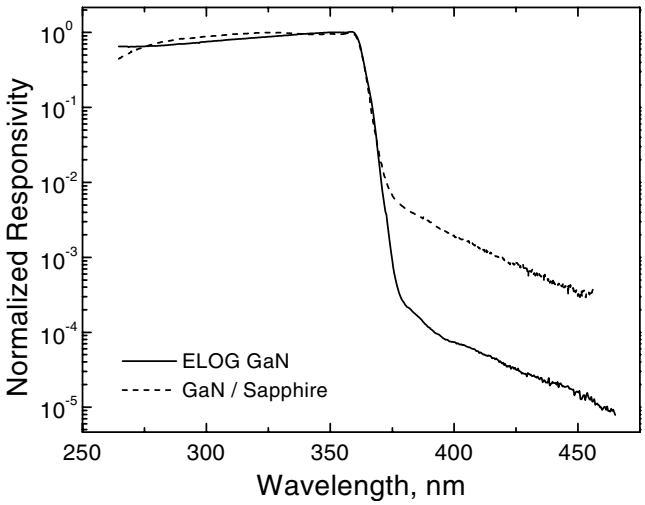

Figure 16. Spectral response of a Schottky photodiode fabricated on ELOG GaN, in comparison with a typical device on standard GaN on sapphire (after [63]).

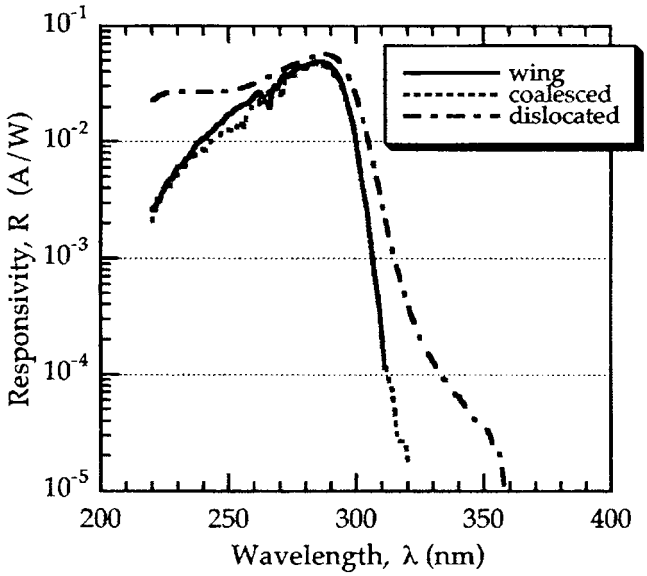

Figure 17. Spectral responsivity of GaN photodiodes fabricated on different regions of a layer grown on ELOG substrate (after [64]).

a peak responsivity at 232 nm, while the device grown on ELOG showed a 30% improvement in responsivity and one order of magnitude higher UV/visible contrast over the detector grown on non-ELOG substrate [65]. GaN MSM detectors grown on ELOG material have been also reported, showing a kind of *hybrid* behaviour [66]. As a complementary experiment, GaN Schottky photodiodes were grown by MBE on HVPE, ELOG-HVPE and sapphire substrates [67]. The spectral responsivity of the devices made on GaN HVPE templates showed a more abrupt cut-off and a higher peak responsivity (50% larger).

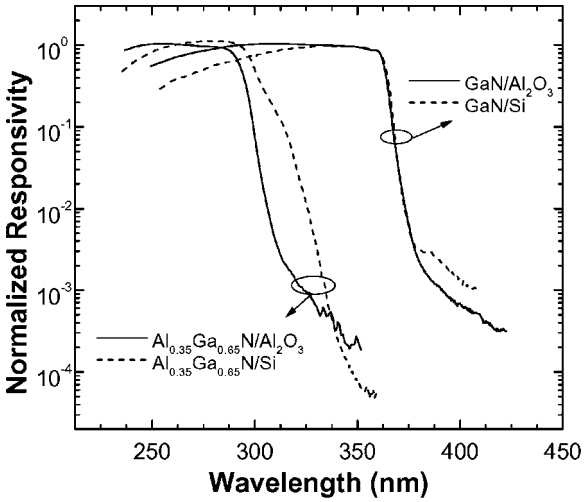

Figure 18. Comparative spectral response of AlGaN Schottky photodiodes grown on sapphire and on silicon substrates.

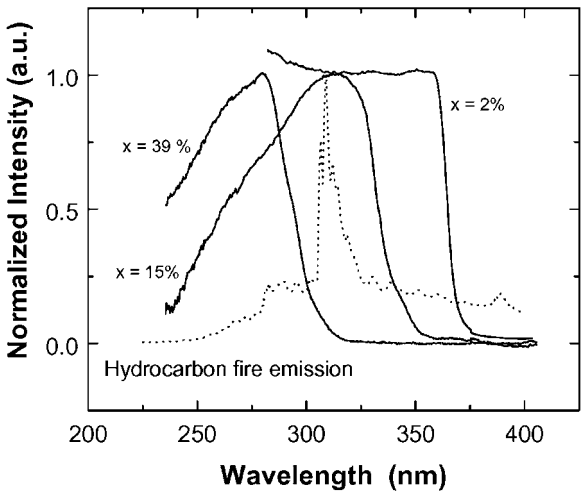

Figure 19. Spectral response of AlGaN MSM photodiodes on Si (111) for Al contents of 2, 15 and 39%. The dotted line represents the typical UV emission from hydrocarbon flames.

The potential advantages of Si⟨111⟩ substrates for nitrides growth have been described in the literature [9, 11, 68–70]. From our experience at ISOM–UPM, the AlGaN layers obtained by GS-MBE do not reach the structural and transport parameters of current state-of-the-art MOVPE on sapphire. The x-ray diffraction measurements show a lower crystalline quality of the AlGaN layers grown on Si (111) by GS-MBE. This higher structural defect density lowers the sensor responsivity and, probably, the carrier diffusion length. However, time response and UV/visible contrast values are close to the best current values found in the literature. Figure 18 illustrates the behaviour at zero bias of Schottky barrier photodetectors grown my GS-MBE on sapphire and on Si substrates. Si substrates allow us to fabricate MSM devices with *hybrid* characteristics, as already indicated. Their contacts are rectifying, with low leakage currents

dominated by tunnelling transport; there is internal gain, without reaching the huge values obtained in AlGaN MOCVD photoconductors. The key for this mixed behaviour seems to be related to the presence of faster recombination centres, as mentioned before [62]. As an example, the use of these devices for flame detection applications is displayed in figure 19, where the MSM detectors have responsivities (optical power <0.1 mW cm^{-2}) evolving from 3.4 A W^{-1} (2% of Al) to 5.2 mA W^{-1} (39% of Al).

7. Conclusions

During the last eight years, AlGaN-based UV photodetectors have been fabricated, showing good responsivity, high UV/vis contrast ratio, high speed and low noise characteristics, and proving the tunability of the detection edge from 360 nm to 225 nm just by varying the Al mole fraction. A linear response is obtained in Schottky barriers, Schottky MSM and p–n junction photodetectors. Sapphire is widely used as substrate, although Si has shown to be also an interesting candidate.

Significant advances in materials quality and device processing techniques have been produced recently. To provide some figures of merit, small area MSM and p–i–n detectors with time responses in the 300 ps range have been reported; solar-blind p–i–n devices with internal quantum efficiencies of 86% have been achieved; very low noise structures with detectivities in the 10^{13} cm W^{-1} Hz$^{1/2}$ range have been fabricated. These high detectivities surpass Si detectors for the UV range. AlGaN photovoltaic devices with sharp UV/visible contrasts between three and five orders of magnitude are obtained today in several laboratories on a standard basis.

The dislocation problem has been shown as one of the most influential and unique in the nitride photodetector behaviour. The use of substrates and growth techniques that decrease the dislocation density in the detector active region directly leads to much lower leakage currents and higher responsivities. The use of lower dislocation density substrates clearly produce lower dark current devices. Dislocations have also been blamed for the low frequency effects that show up in AlGaN photodetectors under certain contact processing and experimental conditions, specially at low illuminating powers.

Although the UV detector market is a bit fragmented, AlGaN devices have shown already their unsurpassed capabilities. Future progress in nitride technology (substrates, materials and processing) will directly benefit AlGaN detector performance and reproducibility. Although it will take some time to have a mature technology, in those applications involving in one way or another the solar UV radiation, AlGaN devices offer today significant advantages over Si detectors, in terms of performance, stability and size (no filter required). Besides, a new era in UV imaging has been opened by focal plane AlGaN photodetector arrays, using p–i–n or MSM devices.

UV imaging, and the simultaneous availability of nitride-based UV sources and photodetectors is going to change drastically some aspects of environmental, medical and biological research and instrumentation, and to open new ways for optical space-to-space and underwater communications.

Acknowledgments

This work was initially supported by the European Union Climate and Environment Program, DG XIII, project ENV4-CT97-0539 (ALDUV). The support of Secretaría de Estado de Universidades e Investigación, project CL198-1359/1660-CE, Comunidad de Madrid project 07M/023/98 and 07M/008/99 and PETRI 95-0466-OP are acknowledged.

References

[1] Muñoz E 1999 *Compound Semicond.* **5** 36–8
[2] Razeghi M and Rogalsky A 1996 *J. Appl. Phys.* **79** 7433–73
[3] Monroy E, Calle F, Muñoz E and Omnés F 2000 *III–V Nitride Semiconductors: Applications and Devices* ed E T Yu and M O Manasreh (New York: Gordon and Breach)
[4] Pankove J I and Berkeyheiser J E 1974 *J. Appl. Phys.* **45** 3892–5
[5] Khan M A, Kuznia J N, Olson D T, Van Hove J M, Blaingame M and Reitz L F 1992 *Appl. Phys. Lett.* **60** 2917–19
[6] Lim B W, Gangopadhyay S, Yang J W, Osinsky A, Chen Q, Anwar M Z and Khan M A 1997 *Electron. Lett.* **33** 633–4
[7] Omnès F, Marenco N, Beaumont B, Mierry Ph De, Monroy E, Calle F and Muñoz E 1999 *J. Appl. Phys.* **86** 5286–92
[8] Sánchez M A, Calleja E, Monroy E, Sánchez F J, Calle F, Muñoz E and Beresford R 1998 *J. Cryst. Growth* **183** 23–30
[9] Brunner D, Angerer H, Bustarett E, Freudenberg F, Hopler R, Dimitrov R, Ambacher O and Stutzmann M 1998 *J. Appl. Phys.* **82** 5090–6
[10] Singh J 1995 *Semiconductor Optoelectronics* (New York: McGraw-Hill)
[11] Stevens K S, Kinniburgh M and Beresford R 1995 *Appl. Phys. Lett.* **66** 3518–20
[12] Walker D, Zhan X, Saxler A, Kung P, Xu J and Razeghi M 1997 *Appl. Phys. Lett.* **70** 949–51
[13] Monroy E, Calle F, Garrido J A, Youinou P, Muñoz E, Omnès F, Beaumont B and Gibart P 1999 *Semicond. Sci. Technol.* **14** 685–9
[14] Reddy C V, Balakrishnan K, Okumura H and Yoshida S 1998 *Appl. Phys. Lett.* **73** 244–6
[15] Kung P, Zhang X, Walker D, Saxler A, Piotrowsky J, Rogalski A and Razeghi M 1995 *Appl. Phys. Lett.* **67** 3792–4
[16] Binet F, Duboz J Y, Rosencher E, Scholz F and Härle V 1996 *Appl. Phys. Lett.* **69** 1202–4
[17] Muñoz E, Monroy E, Garrido J A, Izpura I, Sánchez F J, Sánchez-García M A, Calleja E, Beaumont B and Gibart P 1997 *Appl. Phys. Lett.* **71** 870–2
[18] Garrido J A, Monroy E, Izpura I and Muñoz E 1998 *Semicond. Sci. Technol.* **13** 563–8
[19] Monroy E, Calle F, Muñoz E, Omnés F, Beaumont B and Gibart P 1999 *J. Electron. Mater.* **28** 240–5
[20] Monroy E, Calle F, Muñoz E, Omnés F, Gibart P and Muñoz J A 1998 *Appl. Phys. Lett.* **73** 2146–8
[21] Monroy E, Calle F, Pau J L, Sánchez F J, Muñoz E, Omnès F and Beaumont B 2000 *J. Appl. Phys.* **88** 2081–91
[22] Soares S F 1992 *Japan. J. Appl. Phys.* **31** 210–16
[23] Chen Q, Khan M A, Sun C J and Yang J W 1995 *Electron. Lett.* **31** 1781–2
[24] Walker D, Saxler A, Kung P, Zhang X, Hamilton M, Díaz J and Razeghi M 1998 *Appl. Phys. Lett.* **72** 3303–5
[25] Carrano J C, Li T, Brown D L, Grudowski P A, Eiting C J, Dupuis R D and Campbell J C 1998 *Electron. Lett.* **34** 1779–81
[26] Xu G Y, Salvador A, Kim W, Fan Z, Lu C, Tang H, Morkoç H, Smith G, Estes M, Goldenberg B, Yang W and Krishnankutty S 1997 *Appl. Phys. Lett.* **71** 2154–5
[27] Carrano J C, Grudowski P A, Eiting C J, Dupuis R D and Campbell J C 1997 *Appl. Phys. Lett.* **70** 1992–4
[28] Walker D, Monroy E, Kung P, Wu J, Hammilton M, Sánchez F J, Díaz J and Razeghi M 1999 *Appl. Phys. Lett.* **74** 762–4
[29] Monroy E, Calle F, Muñoz E and Omnès F 1999 *Appl. Phys. Lett.* **74** 3401–3
[30] Monroy E, Calle F, Muñoz E and Omnès F 1999 *Phys. Status Solidi* a **176** 157–61
[31] Carrano J C, Li T, Grudowski P A, Eiting C J, Dupuis R D and Campbell J C 1998 *J. Appl. Phys.* **83** 6148–60
[32] Yang W, Nohava T, Krisnankutty S, Torreano R, Mcpherson S and Marsh H 1998 *Appl. Phys. Lett.* **73** 978–80
[33] Khan M A, Shur M S, Chen Q, Kuznia J N and Sun C J 1995 *Electron. Lett.* **31** 398–400
[34] Li T, Yang B, Beck A L, Collings C J, Yang B, Dupuis R D, Carrano J C M, Schurman J, Ferguson I T and Campbell J C 2000 *SPIE Optoelectron. Tech. Digest* **3948** 304–10
[35] McClintock R, Sandvik P, Mi K, Shahedipour F, Yasan A, Jelen C, Kung P and Razeghi M 2001 *SPIE* at press
[36] Brown J D, Jizhong Li, Srinivasan P, Matthews J and Schetzina J F 2000 *Internet J. Nitride Semicond. Res.* **5** 9
[37] Tarsa E J, Kozodoy P, Ibbetson J, Keller B P, Parish G and Mishra U 2000 *Appl. Phys. Lett.* **77** 316–18
[38] Carrano J, Li T, Eiting C T, Dupuis R D and Campbell J C 1999 *J. Electron. Mater.* **28** 325–33
[39] Yang B, Lambert D J H, Li T, Collings C J, Wong M M, Dupuis R D and Campbell J C 2000 *Electron. Lett.* **36** 1–2
[40] Pernot C, Hirano A, Iwaya M, Detchprohm T, Amano H and Akasaki I 1999 *Phys. Status Solidi* a **176** 147–51
[41] Monroy E, Calle F, Pau J L, Muñoz E and Omnès F 2000 *Electron. Lett.* **36** 2096–8
[42] Monroy E, Calle F, Pau J L, Muñoz E, Omnès F, Beaumont B and Gibart P 2001 *J. Cryst. Growth* **270** 541–7

[43] McIntosh K A, Molnar R J, Mahoney L J, Lightfoot A, Geis M W, Molvar K M, Melngailis I, Aggarwal, Goodhue W D, Choi S S and Spears D L 1999 *Appl. Phys. Lett.* **75** 3485–7
McIntosh K A, Molnar R J, Mahoney L J, Molvar K M, Efremow Y Y Jr and Verghese S 2000 *Appl. Phys. Lett.* **76** 3938–40
[44] Carrano J C, Lambert D J H, Eiting C J, Collings C J, Li T, Wang S, Yang B, Beck A L, Dupuis R D and Campbell J C 2000 *Appl. Phys. Lett.* **76** 924–6
[45] Huang Z C, Mott D B and Shu P K 1998 *AIP Conf. Proc.* **420** 39–43
[46] Brown J D, Yu Z, Matthews J, Harney S, Boney J, Schetzina J F, Benson J D, Dang K W, Terril C, Nohava T, Yang W and Krishnankutty S 1999 *Internet J. Nitride Semicond. Res.* **4** 9
[47] Yang B, Heng K, Li T, Collings C J, Wang S, Dupuis R D, Campbell J C M, Schurman J and Ferguson T I 2000 *IEEE J. Quantum Electron.* **36** 1229–31
[48] Jones R R and Wigley T 1989 *Ozone Depletion: Health and Environmental Consequences* (Chichester: Wiley)
[49] McKinley A F and Diffey B L 1987 *CIE J.* **6** 17–22
[50] Muñoz E, Monroy E, Calle F, Omnès F and Gibart P 2000 *J. Geophys. Res.* **105** 4865–71
[51] Hansen P J, Strausser Y E, Erikson A N, Tarsa E J, Kozodoy P, Brazel E G, Ibbetson J P, Mishra U, Narayanamurti V, DenBaars S P and Speck J S 1998 *Appl. Phys. Lett.* **72** 2247–9
[52] Neugebauer J and Van de Walle C G 1996 *Appl. Phys. Lett.* **69** 503–5
[53] Weimann N G, Eastman L F, Doppalapudi D, Ng H M and Moustakas T 1998 *J. Appl. Phys.* **83** 3656–9
[54] Calleja E, Sánchez F J, Basak D, Sánchez-García M A, Muñoz E, Izpura I, Calle F, Tijero J M G, Sánchez-Rojas J L, Beaumont B, Lorenzini P and Gibart P 1997 *Phys. Rev.* B **55** 4689–94
[55] Hsu J W P, Manfra M J, Lang D V, Richter S, Chu S N G, Sergent A M, Kleiman R N and Pfeiffer L N 2001 *Appl. Phys. Lett.* **78** 1685–7
[56] Hino T, Tomiya S, Miyajima T, Yanashima K, Hashimoto S and Ikeda M 2000 *Appl. Phys. Lett.* **76** 3421–3
[57] Karrer U, Ambacher O and Stutzmann 2000 *Appl. Phys. Lett.* **77** 2012–14
[58] Zhang X, Kung P, Walker D, Piotrowski J, Rogalski A, Saxler A and Razeghi M 1995 *Appl. Phys. Lett.* **67** 2028–30
[59] Pascal D, Hobar-Bourdebous F, Laval S, Bru C, Vilcot J P, Decoster D, Fauquemberge R and Constant M 1985 *Ann. Télécommun.* **40** 3–4
[60] Decorby R G, McDonald R I, Beaudoin M, Pinnington T, Tiedje T and Gouin F 1997 *J. Electron. Mater.* **26** L25–L28
[61] Misra M and Moustakas T D 2000 *Mater. Res. Soc. Symp.* **622** T5.4.1–6
[62] Pau J L, Monroy E, Muñoz E, Naranjo F B, Calle F, Sánchez- García M A and Calleja E 2001 *Electron. Lett.* **37** 239–40
[63] Monroy E, Calle F, Muñoz E, Beaumont B, Omnès F and Gibart P 1999 *Electron. Lett.* **35** 1488–9
[64] Parish G, Keller S, Kozodoy P, Ibbetson J P, Marchand H, Fini P T, Fleischer S B, DenBaars S P, Mishra U K and Tarsa E J 1999 *Appl. Phys. Lett.* **75** 247–9
[65] Sandvik P, Walker D, Kung P, Mi K, Shahedipour F, Kumar V, Zhang X, Díaz J, Jelen C and Razeghi M 2000 *Proc. SPIE* **3948** 265–72
[66] Razeghi M, Sandvik P, Kung P, Walker D, Mi K, Zhang X, Kumar V, Díaz J and Shahedipour F 2000 *Mater. Sci. Eng.* **74** 107–12
[67] Sampath A V, Illiopoulos E, Seth K, Fedyunin Y, Misra M, Ng H M, Lamarre P, Feit Z and Moustakas D 2000 *Proc. SPIE* **3948** 311–19
[68] Osinsky A, Gangopadhyay S, Lim B, Anwar M Z, Khan M A, Kuksenkov D, Temkin H, Shmagin I K, Chang Y C, Muth J F and Kolbas R M 1998 *Appl. Phys. Lett.* **72** 551–3
[69] Pau J L, Monroy E, Naranjo F B, Muñoz E, Calle F, Sánchez García M A and Calleja E 2000 *Appl. Phys. Lett.* **76** 2785–7
[70] Pau J L, Monroy E, Muñoz E, Naranjo F B, Calle F, Sánchez- García M A and Calleja E 2001 *J. Cryst. Growth* **270** 548–52